Measurement of temperature profiles in turbulent pipe flow of polymer and surfactant drag-reducing solutions

K. Gasljevic, G. Aguilar, and E. F. Matthys
Department of Mechanical Engineering, University of California, Santa Barbara, Santa Barbara, California 93106, USA

(Received 19 May 2006; accepted 19 July 2007; published online 29 August 2007)

A device was built to measure temperature profiles of turbulent pipe flows of various drag-reducing fluids. It is easy to use and reliable. We measured temperature profiles over a range of conditions leading to accurate measurements down to $y^+ \approx 10$, for tests carried over Reynolds numbers (Re) between 10 000 and 90 000. The effects of high heat fluxes and buoyancy, in particular, were quantified to ascertain the parameter range for accurate measurements. Temperature profiles measured for type-A polymer solution and for cationic surfactant solutions allowed us to see strong similarity between velocity and temperature profiles for drag-reducing surfactant solutions. A comparison between the slopes of the thermal and velocity buffer layers resulted in calculated turbulent Prandtl numbers between 6 and 9 for those drag-reducing solutions. We also used this tool to investigate drag reduction for a nonionic surfactant solution, which showed a significantly different fan-type profile, and also for a type-B drag-reducing polymer solution (Xanthan gum).
 [DOI: 10.1063/1.2770257]

I. INTRODUCTION AND LITERATURE REVIEW

The drag reduction (DR) phenomenon is well-known. It is characterized by a dramatic reduction of friction in turbulent flow that can be achieved through the addition of very small quantities of drag-reducing additives to water. It is customary to express drag reduction numerically as

$$\mathrm{DR} = 100 \times \left(1 - \frac{c_f}{c_{f,w}}\right) [\%], \tag{1}$$

where c_f and $c_{f,w}$ stand for the friction coefficient of the drag-reducing solution and the friction coefficient of the pure solvent (e.g., water), respectively, at the same Reynolds number. Only a few parts per million of the most efficient drag-reducing additives, such as high-molecular-weight polymers, can reduce turbulent friction in pipes by as much as 80%. Significantly higher concentrations are needed for the same level of drag reduction, however, if surfactants, another class of widely used drag-reducing additives, are used.

Although the major phenomenological laws of drag reduction based on global measurements of turbulent phenomena were established some time ago,[1] improved measurements—facilitated by the use of laser Doppler velocimetry (LDV)—were achieved more recently (addressed below in more detail). Those measurements confirmed to a large extent Virk's velocity profile for drag-reducing solutions and an almost full disappearance of the Reynolds stresses at maximum drag reduction that is partially compensated for by the appearance of elastic stresses. Velocity fluctuations normal to the wall were found strongly dampened, while streamwise velocity fluctuations were increased.

More recently still, continuum-level simulations offered valuable information about turbulence in drag-reducing flows (i.e., its effect on mean velocity profile, turbulence, and elastic stresses, and different turbulence statistics). A commonly used model for drag-reducing polymer solutions is the FENE Peterlin model,[2] in which a polymer chain is represented by a dumbbell consisting of two beads connected with a spring. The Oldroyed-B model has been used as well.[3] Those models allow a coupling between polymer and flow in two ways; the polymer is deformed by the flow and the resulting stress in turn contributes to the stresses in the flow. The results of those simulations are generally in good qualitative agreement with experimental observations. Yu and Kawaguchi[4] applied the Giesekus viscoelastic constitutive equation to drag-reducing surfactant solutions to model the interaction between the elastic network and flow. High levels of drag reduction of up to 72% were achieved. They found that the occurrence of large drag reduction requires large elastic energy in a wide buffer layer (fluid with large relaxation time, i.e., Weber number, a large mobility factor (effects elongational viscosity) and a large solvent-to-solution viscosity ratio.

Two main theoretical concepts have been proposed to explain drag reduction by additives. The first suggested by Lumley[5] is based on the observation that randomly coiled polymer molecules stretch in regions of strong deformation, increasing the extensional viscosity of the solution. This in turn results in damping of small turbulent eddies; i.e., reduction of Reynolds stresses and reduction of drag. The second mechanism, offered by de Gennes[6] relies on the elastic character of the drag-reducing solutions, which can store elastic energy in polymer molecules and lead to modifications of the turbulent cascade when the elastic stresses become comparable to the Reynolds stresses. The shear waves caused by the elasticity of the solution could then prevent production of fluctuations at the Kolmogorov scale.

Drag reduction is accompanied by an even higher level

of heat transfer reduction. Similarly to the quantification of drag reduction, heat transfer reduction can be expressed as

$$\mathrm{HTR} = 100 \times \left(1 - \frac{\mathrm{Nu}}{\mathrm{Nu}_w}\right) [\%] \tag{2}$$

where Nu and Nu_w stand, respectively, for the Nusselt number of the drag-reducing solution and the Nusselt number of the pure solvent (water in our case). Better quantification parameters do exist,[7] but will not be used here for simplicity. Aguilar *et al.*[8] found that the ratio of HTR to DR in straight pipes is a weak function of the Reynolds number (i.e., of the flow velocity). The HTR-to-DR ratio decreases with increasing Reynolds number, stabilizing at a value of 1.14 for Reynolds numbers above 10^4. (If one uses the improved parameters mentioned above, the ratios are essentially independent of the Reynolds number.)

Modern and accurate methods for velocity measurements, such as laser Doppler velocimetry and particle image velocimetry, have been used successfully in the determination of the velocity profiles of Newtonian flows as well as of turbulent drag-reducing flows. Velocity profile measurements of turbulent drag-reducing flows have provided most of the experimental evidence used for developing the phenomenological interpretations of drag reduction for both polymer and surfactant solutions. Measurements of velocity fluctuations and their correlations allowed indeed for descriptions of drag reduction as a result of reduced Reynolds stresses, as well as through identification of an elastic stress associated with elastic properties of the drag-reducing solutions. Through velocity profile measurements it has also been possible to calculate directly the values of the diffusivity coefficients of momentum (ε_M).

For simple turbulent flows of Newtonian fluids, the Reynolds and Colburn analogies successfully relate momentum and heat transfer, resulting in similarity of temperature and velocity profiles. The simplest and surprisingly adequate turbulence model based on the Prandtl mixing length, does quantify the turbulent heat diffusion by relating the momentum and heat eddy diffusivities through the use of the turbulent Prandtl number. This parameter does not deviate much from unity, both for simple flows over a plate and also for pressure gradient-driven developed flows in channels.[9]

It was long thought, however, that for drag-reducing turbulent flows, an analogy between momentum and heat transfer does not hold. Indeed, drag-reducing additives produce higher levels of heat transfer reduction than of drag reduction. Heat transfer being affected more by drag-reducing additives than momentum transfer suggests that the turbulent Prandtl number for drag-reducing flows may be significantly higher than unity. It was also thought earlier that the momentum entry length for polymeric in drag-reducing pipe flows is about 120 diameters, whereas as much as 500 to 1000 diameters are needed for a steady level of heat transfer to be reached. Cho and Hartnett[10] calculated different diffusivities for mass, momentum, and heat—decreasing in that order—for drag-reducing flows, based on the increasing mass, momentum, and heat transfer entry lengths. More recently, however, it was shown[11] that the development of momentum and heat transfer layers in drag-reducing flows take place simultaneously, for both nondegraded surfactant solutions as well as for surfactant solutions recovering after degradation by mechanical stress

Based on known velocity profiles, different expressions were offered for the calculation of diffusivity coefficients for momentum (ε_M) in drag-reducing pipe flow.[10,12,13] For asymptotic drag reduction, all those expressions give relatively consistent values of ε_M as a function of nondimensional distance from the wall. Knowing the experimentally established relationships between drag and heat transfer reductions, one can then also estimate the diffusivity of heat (ε_H), relate it to diffusivity of momentum, and then calculate the value of the corresponding turbulent Prandtl number. Cho and Hartnett[10] and Yoon and Ghajar[13] offered expressions for the diffusivity of heat, analogous to their predictions of diffusivity of momentum. Roethig and Matthys[14] then calculated the turbulent Prandtl number as a function of Reynolds number, including Mizushina's and Usui's model for ε_M and calculating ε_H by matching experimentally obtained values of drag and heat reductions. Using the model proposed by Mizushina and Usui led to a Pr_t of 11.8, practically independent on Re, whereas the other two models provided values varying between 10 and 15, depending on the Reynolds number. Generally, the turbulent Prandtl number estimates were much higher than the values near unity that are typical of Newtonian fluids.

Using this approach it is not possible to differentiate—at least without a large uncertainty—the overall contribution of the laminar and turbulent diffusivity coefficients to the temperature profiles. Therefore, the inaccuracies associated with the determination of the Pr_t could be reduced if the velocity and temperature profiles were measured directly and simultaneously, but only a few measurements of the temperature profiles of drag-reducing fluids have apparently been conducted until now. Resolving the issue of the value of the Pr_t for drag-reducing fluids may lead to a better understanding of the drag reduction phenomenon and also provide a better insight into the turbulence phenomena in general.

Measurements of the temperature profiles for a variety of drag-reducing fluids under different flow conditions may also offer an alternative to the velocity profile measurements used until now for identifying different types of drag reduction. It was recognized recently that drag reduction may also involve velocity profiles different from Virk's velocity model, with the drag-reducing effects not being limited to the elastic layer, but spreading to the core of the flow, even for drag-reducing flows which are not asymptotic.[15,16] The temperature profile measurements may indeed have advantages in some cases over the velocity profiles for characterization purposes, as will be discussed below.

A. Velocity profile measurements for polymer solutions

Velocity profile measurements for drag-reducing polymer solutions were originally carried out using Pitot tubes. Based on a large database of velocity profile measurements made by several investigators for various polymer solutions

under different flow conditions, Virk *et al.*[1] proposed what is perhaps the best known velocity profile model for drag-reducing fluids: the three-layer model. This model consists of a viscous sublayer and a turbulent core (as for Newtonian fluids), plus an elastic or buffer layer between these two, the buffer layer being presumably where most of the drag-reducing effects take place. As the level of drag reduction increases, this layer thickens, reducing the size of the turbulent core layer. This model was tested experimentally thereafter by other researchers[17,18] and showed reasonably good agreement with measurements.

Later on, more accurate techniques for velocity measurements were developed. The most common ones are laser Doppler velocimetry and particle tracking techniques such as particle image velocimetry, and a number of studies were conducted in which velocity profiles have been measured using these techniques is a relatively long one. Perhaps some of the first thorough measurements using such techniques were conducted by Reichman and Tiederman,[19] who conducted systematic LDV measurements of drag-reducing channel flows and showed slight variations with respect to Virk's three-layer model. They concluded that there was no evidence of viscous sublayer thickening, but rather that the drag reduction results from a growth of the buffer layer, and that the buffer layer did not follow a fixed slope in the u^+-y^+ coordinates, as proposed by Virk, but instead varied somewhat with the level of DR.

Other techniques have also been used. Li and McCarthy[20] used nuclear magnetic resonance imaging to measure pipe flows of various polyacrylamide solutions. Like the Reichman and Tiederman experiments, their results for a 200 ppm polyacrylamide solution show a slightly increased slope of the logarithmic layer, but, qualitatively, their results are very close to Virk's three-layer model. More recent measurements with LDV[21] also agree reasonably well with Virk's three-layer model.

Overall, despite the variations in the velocity profiles that some researchers have pointed out with respect to Virk's three-layer model, most of the reported data seem to agree reasonably well with this model. In any case, if those variations were to be considered and incorporated into the model, they would not have a large effect on the overall drag reduction estimates, though they would add complications to the calculation procedures. This is why most researchers have used Virk's three-layer model, and so will we for the analyses of the polymer solutions data presented in this work.

B. Velocity profile measurements for surfactant solutions

As the use of surfactants as drag-reducing fluids has become more attractive, the velocity profiles for these fluids have been studied increasingly. The velocity profiles for surfactant solutions[22,23] exhibit a viscous sublayer and a Newtonian turbulent core as do Newtonian fluids and polymer solutions. They also exhibit a buffer layer, like polymer solutions, but with a slope of about twice that of polymer solutions. In the turbulent core region, some surfactant solutions show profiles identical to the Newtonian logarithmic layer, though other profiles show an increased slope relative to the Newtonian case. Similar characteristics of the velocity profiles were also reported by Bewersdorff and Ohlendorf[16] for surfactant solutions measured in pipe flows. It has been suggested[24,25] that this change in the pattern of the core region of the profiles is associated with an increase of the shear-dependent viscosity of the surfactant solutions. The evaluation of local viscosity is a complicated issue with surfactant solutions, however, as these typically show an increased viscosity compared to water (unlike most low concentration polymer solutions), and also a viscosity that may be a strong function of flow history. To address this issue to some extent, Bewersdorff and Berman[26] used a viscosity obtained with a capillary viscometer, together with velocity profile gradients, to calculate a "variable local viscosity." In this way, they showed that velocity profiles exhibiting apparently lower nondimensional velocities in the buffer zone could be shifted by this procedure, and thus resemble more the typical asymptotic profiles for polymer solutions as in Virk's three-layer model.

Despite the variations in the proposed velocity profiles in the nonasymptotic regime (and therefore in the frictional behavior) of surfactant solutions that appear in the literature, it is generally agreed that there exists an asymptotic profile for surfactant solutions, analogous to that for polymer solutions, but corresponding to higher levels of drag reduction. For example, Zakin *et al.*[27] have gathered data from various authors and have suggested an asymptote for surfactant solutions. In terms of the velocity profiles, this asymptotic profile shows an slope of the buffer layer increased by a factor of 2 with respect to Virk's asymptotic profile. It is interesting that these surfactant solutions still show some Newtonian logarithmic layer close to the pipe center, even when maximum asymptotic conditions have presumably been reached. This was also noted by Bewersdorff and Ohlendorf.[16] Other correlations for related asymptotic friction and heat transfer have also been proposed.[28]

C. Temperature profile measurements

Regarding measurements of turbulent temperature profiles, there was significantly less work done for viscoelastic fluids than for Newtonian fluids. On the Newtonian side, the experiments along a flat plate for air[29] and water[30] suggest that the Pr_t tends to approach a constant value of about 0.85 in the far-from-the-wall region (beyond $y^+=30$). However, in both cases (for $\mathrm{Pr}=0.7$ and 5.9, respectively), the Pr_t increases to about 2 closer to the wall (at a y^+ of about 6). Similarly, temperature profile measurements[31] conducted for the region beyond $y^+=30$, show a reasonably good agreement with a law-of-the-wall equation of the form $T^+=2.075 \ln y^+ + 7.55\ \mathrm{Pr}^{2/3} - 3.95$, in which the Pr_t was assumed to be 0.85. It is important to point out that they reported the temperature measurement closest to the wall at $y^+=3.5$, and that up to a $y^+=6$, the thermal sublayer is well represented by the linear equation $T^+=\mathrm{Pr}\, y^+$.

Interestingly, despite the sophisticated techniques that have been developed recently for the measurement of temperature, thermocouple sensors are still used for the vast ma-

jority of temperature measurements in fluid dynamic and heat transfer experimental setups. Modern technologies, such as liquid crystal thermography, have provided new tools for temperature measurements through color visualization, but their use in three-dimensional flows is difficult.

In contrast to Newtonian fluids, the work done on turbulent temperature profiles for polymer and surfactant solutions is very limited. Perhaps the first attempt was made by Khabakpasheva and Perepelitsa.[32] They measured simultaneously the velocity and temperature profiles for aqueous polyacrylamide solutions in a square channel flow and estimated the eddy diffusivities of momentum and heat for these drag-reducing flows. They found that the Pr_t exceeded a value of 1 over a substantial portion of the test cross section, and that it had an average value between 2 and 3, which is much lower than the Pr_t predicted by diffusivity models based on the overall heat transfer coefficients[10,12–14] which typically give values of Pr_t between 10 and 15.

More recently, Kawaguchi *et al.*[33] reported a series of temperature profile measurements for surfactant solutions such as (cetyltrimethylammonium cloride/sodium salycilate) CTAC/NaSal. Interestingly, their measurements showed what they called a *double diffusivity fluid layer*, meaning a region of high diffusivity close to the wall, followed by a region of low diffusivity (corresponding to a buffer layer). This behavior was explained by the action of buoyancy effects (being dominant in the region close to the wall), combined with the suppression of the drag-reducing effectiveness of the fluid in the same region due to the change of the rheological fluid properties with temperature. Li *et al.*[34] measured not only the temperature and velocity profiles for the flow of a drag-reducing surfactant solution in a channel, but also temperature and velocity fluctuations. Based on those measurements, they calculated the turbulent Prandtl number as a function of distance from the wall. This was a determination of the turbulent Prandtl number for drag-reducing flows based on measured Reynolds stress and turbulent radial heat flux. They found that the turbulent Prandtl number for drag-reducing fluid was increased relative to a Newtonian fluid only in the region close to the wall, below $y^+=50$, whereas for distances further from the wall the turbulent Prandtl number was about 0.9 for both drag-reducing and Newtonian fluids.

Aguilar[1] and Gasljevic *et al.*[35] used temperature profile measurements to support the proposed concept of two distinct types of pipe diameter effects on drag reduction exhibited by two types of surfactant solutions (cationic and nonionic).

We know only of one study dealing with numerical simulation of the temperature field in drag-reducing flows. Using the (finitely-extensible-nonlinear-elastic) FENE-Peterlin constitutive equation, Gupta *et al.*[36] solved the unsteady three-dimensional equations for mass and momentum conservation, viscoelastic stress, and passive scalar (temperature) transport. The three parameters influencing drag and heat transfer reductions were relaxation time, molecular flexibility and the ratio of solvent to solution viscosity. The eddy diffusivity for heat as a function of the distance from the wall was found to be similar to the eddy diffusivity for momentum, showing an overall decrease with increasing level of drag reduction, this similarity resulting from similar behaviors of the velocity and temperature fluctuations. However, whereas the eddy diffusivity for momentum showed a strong decrease further from the wall after reaching a maximum, the decrease was much smaller for the eddy diffusivity of heat. Consequently the turbulent Prandtl number varied with the distance from the wall. For the highest modeled level of drag reduction of 52.5%, the highest level of turbulent Prandtl number calculated by the wall was 24, whereas towards the center of the channel it dropped to about the value of the molecular Prandtl number; i.e., 6. The normalized (with respect to the Newtonian values) ratio of Colburn factors for heat and friction j_H/j_F was a strong function of drag reduction, varying from 1 at DR=0 to 0.3 at DR=75. This contrasts with the measurements of the ratio of heat and drag reductions conducted by Aguilar *et al.*, which showed an approximately constant value of 1.1, independent of the level of drag reduction.

II. EXPERIMENTAL SETUP AND PROCEDURES

In the research project discussed in this article, we addressed a wide range of issues related to drag-reducing flows by means of temperature profile measurements. Although the issue of turbulent Prandtl number may be the first one which comes to one's mind as an unresolved problem for drag-reducing flows that is likely to benefit from temperature profile measurements, there are others as well. As mentioned above, there is strong evidence, based on velocity profile measurements as well as drag reduction measurements in pipes of different diameters, that the general phenomenology of drag reduction for different types of drag-reducing additives may differ for each type. If a general relationship between velocity and temperature profiles of drag-reducing flows can be established, one could use temperature profiles instead of velocity profiles to classify drag-reducing flows. One advantage of such an approach is that temperature profile measurements may be more accurate in some cases than velocity profile measurements. In any case, temperature profile measurements can also shed light on the phenomenology of drag-reducing flows, which until now was based exclusively on the velocity profile measurements. The latter, although numerous, still offer contradictions regarding such issues as viscous sublayer thickening, variable slopes of buffer layer, and the presence of the Newtonian core region.

To accomplish this goal, we built an experimental setup that allowed reliable and relatively simple measurement of temperature profiles. The flow channel was a stainless steel tube of 19.95 mm inner diameter. The circular cross section of the channel—rather than a square one—improved radial symmetry of the flow, and allowed a relatively smaller cross section of the channel, because of the elimination of the corner effects present in the square geometry. Consequently, the flow rates at a given flow velocity were kept low, as were the amounts of solutions to be prepared. This was important, because we intended to test a larger number of drag-reducing solutions, at different concentrations and flow velocities. This tube flow geometry also allowed for symmetrical radial

heat flux, long entry region (thanks to a relatively small cross section) to ensure fully developed conditions regarding friction and heat transfer, as well as easy and accurate drag and heat transfer reduction measurements. The circular cross section of the flow channel did impose a strict requirement of temperature probe alignment with the flow direction, however. (The probe was L-shaped and the distance from the wall to the temperature sensor, placed on the tip of the probe, was very sensitive to this alignment, particularly at locations close to the wall.)

A. Flow loop and global friction and heat transfer coefficient measurements

Avoiding mechanical degradation was a major concern for most of our experiments, and various design requirements and procedures were implemented for this purpose. First, the concentrated polymer solutions were gently poured and mixed in water for several minutes. The solutions were then allowed to rest in the tank for a minimum of 24 h, so that small lumps of concentrated polymer (or surfactant) would be completely dissolved. Later, the fluid was slowly fed by gravity from a 1 m^3 plastic tank into a large 2.5 m^3 closed steel tank. This steel tank could then be pressurized by up to 7 bar to drive the solutions through the tubes. PVC feed pipelines of relatively large inner diameter compared to the test pipe, were then used to minimize mechanical (and possibly chemical) degradation during the run.

The test pipe was built of 304 stainless steel and had a calibrated inner diameter of 19.95 mm. It could be fed by the pressurized tank or, alternatively, by centrifugal variable-speed pumps (3 and 7.5 HP). The large 2.5 m^3 volume of the supply tank ensured a negligible change in the pressure in the tank during the test runs, so that a practically constant flow velocity could be maintained. When a fluid was fed by the pump, it first passed through a 15 m long pipe of a 52 mm diameter, prior to reaching the test tube, so that it could recover from any mechanical degradation which may have occurred in the pump. The length-to-diameter ratio of the test tube was 680.

Very smooth and uniform pressure tap holes are essential to avoid viscoelastic hole pressure errors when measuring the pressure drop in the tube, and these holes were therefore drilled by electric discharge machining. The pressure drop measurements were taken by Validyne DP 15 variable-reluctance differential-pressure transducers. To ensure hydrodynamic and thermally fully developed conditions, the pressure drop and temperature measurements were taken as far downstream from the tube entrance as possible, typically between 630D and 6675D. Adjacent upstream pressure drop measurements were also taken to check for fully developed conditions.

We used the once-through mode for all tests, meaning that the fluid made only one pass through the test tube during a run, again to avoid degradation. Depending on the test conditions and the expected flow rate, one of two calibrated tanks (of 0.1 and 0.30 m inner diameter) were used to collect the fluid at the end of the test pipe. Continuous measurement of the height of the collected fluid (via hydrostatic pressure) during a run was used for the calculation of the flow rate. This procedure is the simplest and perhaps the most accurate bulk velocity measurement for viscoelastic fluids (about 1% accurate in this case).

For the heat transfer reduction measurements, the test tube was instrumented with six temperature sensors (miniature RTDs 10×2 mm, 100 Ω) cemented on the outer wall of the test tube, three at 634 diameters, and another three at 675 diameters from the tube entrance. The three RTD sensors placed at each longitudinal location on the test tube were located at the top, bottom, and side of the tube to provide redundancy for the tube wall temperature measurements and to allow the detection of possible buoyancy effects on the heat transfer measurements. Another RTD (shielded probe, 100 Ω) was inserted perpendicular to the flow in the supply manifold of the pipe, for inlet fluid temperature measurements. A two-wire configuration was used to measure the RTD resistances by a high-accuracy, multichannel, digital multimeter (Keithley 199). Short and thick connecting wires were used to minimize the wires-to-RTD resistance ratio. The constant wall heat flux heating was provided by two Hobart 20 kW DC power supplies connected in parallel, which could provide currents of up to 1000 A, by passing the current lengthwise through the wall of the test tube. To minimize the contact resistance at the points of connection between current carrying cables and the test tube, two precisely machined clamps were coated with a 0.2 mm thick layer of soldering tin, which when tightened accommodated to the shape of the test tube eliminating possible air gaps. To avoid heat losses, two layers of polyurethane pipe insulation covered the pipe all the way from the entrance to the discharge.

Data collection for all pressure drop and flow rate measurements and both voltage and current inputs, was achieved by a Validyne UPC608 data acquisition card. The acquisition control was handled by Labtech Notebook software. All temperature measurements were taken and temporarily stored in the standalone Keithley 199 digital multimeter.

B. Temperature profile measurements

The choice of appropriate sensors was determined mostly by size requirements. RTDs were preferred over thermocouples for the wall temperature measurements because of lower noise pickup. However, the smallest sizes of commercially available RTDs are many times larger than sensors one can obtain (or fabricate) using thermocouple wires. This is an important issue for the temperature profile measurement. Two devices for fluid temperature measurements were therefore built with thermocouples, differing in the way the thermocouple wires were attached to their support. All sensors used were homemade type E (Chromel™-Constantan) that provided the largest response ($\approx$60 mV/°C) possible. The choice of the wire thickness was an important design consideration. On the one hand, a small sensor tip (or bead) is needed to ensure high resolution for the temperature measurements, as well as to minimize disturbances to the flow. On the other hand, the noise pickup is proportional to the wire resistance, which in turn increases inversely proportionally with the square of the cross-sectional area. Therefore, a

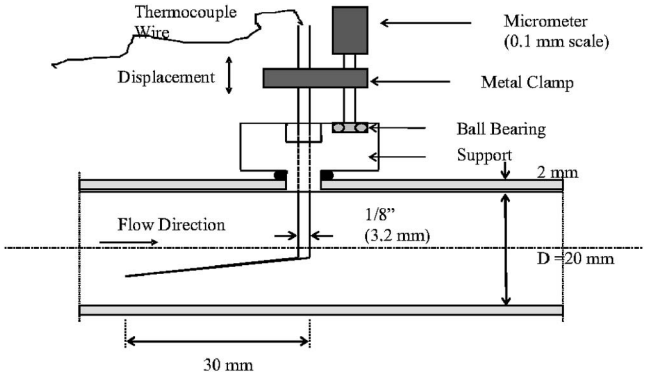

FIG. 1. Temperature sensor design and location in the test tube (not to scale).

very tiny wire would have been a bad choice considering the noisy environment that the currents of up to 1000 A used for heating the tube could generate, and also because very small sizes would have been difficult to handle. Wires of 0.003 in. (0.0076 mm) diameter were decided on as the best compromise. This wire thickness also provided enough rigidity to the sensor tip, so no additional support was needed as will be described below.

Two devices for temperature profile measurements were built and tested. One was made from a thin mica sheet, spanning the diameter of the test tube, with 15 thermocouple sensors attached to it across the radius of the tube, spaced in uniform increments starting at 0.25 mm from the wall. All 15 temperature sensors could be scanned simultaneously. The other device contained only one temperature sensor, placed at the tip of a thin tube of 0.7 mm diameter. This sensor was moved across the pipe during a run, and temperature measurements were taken at each location. After numerous tests the second device was found to provide better temperature profile measurements, mostly due to lesser disturbance to the flow—particularly in the region close to the wall—and adjustable location, although at the price of a more tedious experimental procedure. All temperature profiles reported in this paper were measured using this latter device.

This device is based on a thermocouple junction of type E with leads of 0.003 in. (0.076 mm) thick, and a bead of approximately spherical shape with a mean diameter of about 0.007 to 0.008 in. (0.17 mm). A sketch of this arrangement is shown in Fig. 1. In order to avoid the effect of large disturbances to the flow, the sensor bead had to protrude upstream of the horizontal support tube. A protrusion of 1 to 2 mm was found to be satisfactory, both in order to assure that the wires had enough rigidity to keep the sensor at a fixed position in the flow, and to avoid the risk of short-circuiting the wires electrically through the fluid. To strengthen and electrically insulate the wires, a thin coat of glue was applied to them. The bottom of the bead was kept free of the glue, however, to allow for an electrical contact with the wall during the calibration of the sensor position (see below).

Finally, the support tube was attached to a vertical traverse brass tube (of 3.2 mm diameter) at a small angle (about 15°) relative to the horizontal (see Fig. 1). This small angle was chosen as a compromise between two requirements. On the one hand, the disturbance to the flow due to the relatively bulky tubing right behind the sensor was minimized by its nearly horizontal position. On the other hand, the calibration of the sensor positioning was made simpler by having this angle larger.

Other provisions were also taken to minimize electrical noise. For instance, extension thermocouple wires were kept short and were made of larger diameter than the short wire used for the tip of the thermocouple. Two thermocouples measuring the wall-to-local temperature difference $T_w - T(r)]$ were connected in series to increase common mode noise rejection. With this arrangement, not only was one voltage output eliminated, but the measured voltage was also directly proportional to $T_w - T(r)$; i.e., the temperature difference used for constructing the temperature profiles. Finally, since only the average mean temperature was of interest, the temperature fluctuations of the signal were filtered by the built-in running-average filter of the digital multimeter used for the data acquisition (Keithley 199 DMM/Scanner).

C. Test procedure

To avoid the need for simultaneous measurements of velocity and temperature profiles, we took advantage of the existence of a large number of velocity profile measurements that have been obtained in the past for certain drag-reducing solutions. We used some well-established velocity profile models in combination with our drag reduction, heat transfer reduction, and temperature profile measurements to investigate the possible similarity of velocity and temperature profiles, and to obtain estimations of the turbulent Prandtl number (Pr_t). This procedure was only followed for those fluids with well-documented velocity profiles; namely, drag-reducing solutions that conform to Virk's three-layer model.

First, we tested polymer solutions with well-known velocity profiles. One was a polyacrylamide solution (Separan™ AP-273, a product of Dow Chemical), which is well represented by the three-layer velocity profile model.[1] Similarly, the velocity profiles of some cationic surfactant solutions have been established[22,27] showing a steeper slope of the buffer layer compared to polymer solutions and a somewhat larger sublayer thickness (which seems to be a consequence of the increased slope of the buffer layer). As mentioned above, simultaneous global measurements of DR and HTR were taken together with the temperature profile measurements. From the drag reduction measurements and the three-layer velocity model, an estimated velocity profile was then calculated. Note that an accurate drag reduction quantification (based on two redundant measurements of pressure drop), together with the three-layer model (proved valid by many measurements by different authors), may likely provide more trustworthy information on the velocity profile than a single velocity profile measurement done simultaneously with the temperature profile measurement could, since large errors can be made in measuring local velocities. This estimated velocity profile was then used, together with the temperature profile, to compute an corre-

sponding overall heat transfer coefficient or the heat transfer reduction HTR. As the heat transfer reduction was also directly calculated from the global measurements (tube wall temperature and bulk fluid temperature), a comparison with the heat transfer measurement based on the temperature profile can be made. We found a good match between the global HTR measurements and the heat transfer coefficients computed through the integration of the temperature and velocity profiles. This good match—typically within 3%—suggests that the procedure is appropriate. We used the cationic surfactant Ethoquad® T13-27 (a product of AKZO Chemicals), which is a tris (2-hydroxy-ethyl) tallowalkyl ammonium acetate, with sodium salicylate(NaSal) as a counter-ion, for these experiments.

Once we had both temperature and velocity profiles (for the fluids which conform to the three-layer velocity profile), the similarity of the velocity and temperature profiles was examined. As will be discussed below, the similarity of the profiles allowed us to generate estimates for the turbulent Prandtl number. Since velocity and temperature fluctuations were not directly measured, we assumed that momentum and heat eddy diffusivities are not a function of location in the buffer layers of the velocity and temperature profiles. The assumption of constant eddy diffusivities in the logarithmic buffer regions of the velocity and temperature profiles is not exactly correct for pressure-driven channel flow, but may still be acceptable because in drag-reducing flows we are expecting an average turbulent Prandtl number of the order of 10, rather than 1 as is the case for Newtonian fluids, and the error due to the incorrect assumption of constant eddy diffusivities will not be too severe.

For the fluids for which there is no velocity profile available, the temperature profile measurements, along with the overall HTR/DR ratio measurements, were used to determine the characteristics of the velocity profiles, based on the assumption of a similarity between the velocity and temperature profiles.[35] Following this procedure, we have determined that some temperature profiles and, thus, their corresponding velocity profiles may be in some cases very different from those described by the three-layer model. Those temperature profiles allowed us to investigate some important aspects of the drag reduction phenomenon, particularly those that cannot be explained in more detail through global friction and heat transfer coefficient measurements alone. Those are, for example, the existence of different drag-reducing mechanisms, the difference in the diameter effect between different solutions, the effect of contaminants on the diffusivity coefficients, etc. Therefore, the temperature profiles can become as powerful a tool for the analysis of certain aspects of the drag reduction phenomenology as the velocity profiles are, and in some cases even better. Two drag-reducing additives were used in this category of tests, with unknown velocity profiles: a biodegradable nonionic surfactant (SPE95285) and the biopolymer Xanthan gum. The nonionic surfactant SPE95285, a proprietary mixture of two surfactants, was developed by AKZO-Nobel Chemicals for us as a drag-reducing additive for low temperatures. Some information on its composition can be found in Ref. 35. The polymer Xanthan gum we used is a polysaccharide manufactured by Kelco Corp. by aerobic fermentation with the bacteria *Xanthomonas campestris*.

To obtain the temperature profile measurements, the bulk velocity was usually maintained between 1 and 2 m/s for this particular diameter pipe, corresponding to Reynolds numbers between 20 000 and 40 000 for fluids with water-like viscosity at room temperature conditions (for fluids with higher viscosity, the velocity was increased). Several objectives were achieved by this choice. First, ensuring a large enough Reynolds numbers for the experiments to be carried out beyond the transition region from laminar to turbulent flow, but, at the same time, not so large that the dynamic force exerted by the fluid on the sensor could produce mechanical oscillations. On the other hand, a relatively low Reynolds number allowed for proportionally thicker viscous and thermal sublayers, and thus permitted better resolution in the region close to the wall (i.e., obtaining measurements at a lower y^+). Furthermore, the range of velocities between 1 and 2 m/s happens to be the range of interest for many practical applications. Nevertheless, for some runs the Reynolds number was increased up to 100 000.

The wall heat flux (q''_w) was controlled so as to maintain a wall-to-bulk temperature difference ($\Delta T_{w\text{-}b}$) of about 2 °C for most tests. With this temperature difference, the effect of the radial temperature variation on the fluid viscosity was not more than 4% for average test conditions, and much less for other thermophysical properties such as heat capacity and density. For most drag-reducing fluids, the effect of this temperature variation on their drag-reducing ability was negligible as well. However, perhaps the most important reason for keeping the $\Delta T_{w\text{-}b}$ small was to avoid possible large distortions of the flow due to natural convection.[37]

The fluid viscosity (μ) was an important parameter to consider for shear-thinning drag-reducing solutions. On the one hand, the uncertainty in defining the viscosity at different locations in a varying velocity field makes fluids with water-like viscosity the best choice. On the other hand, a fluid with higher viscosity provided thicker viscous and thermal sublayers at the same flow conditions, which in principle offers the opportunity to obtain measurements in the near-wall region. It was decided that it was most important for our purposes to focus on the accuracy of the Pr_t measurements, and the fluid viscosity was therefore kept as close as possible to water for most runs, except in some special cases where the effect of an increased viscosity was either desirable (e.g., in tests of the temperature sensor in the laminar flow) or unavoidable (for the Xanthan gum solution).

To determine the position of the sensor inside the pipe, a 12 V AC transformer was connected to the thermocouple and to the test tube, using each as an electrode. The thermocouple was then moved towards the wall of the (empty) pipe, and the point of contact (at $y=0$) was detected by the closed electrical circuit. AC voltage was chosen for this purpose rather than DC to avoid possible polarization of small residues of liquid that could affect the repeatability of the electrical resistance readings at the contact position and in turn result then in bent probe and inaccurate height measurements.

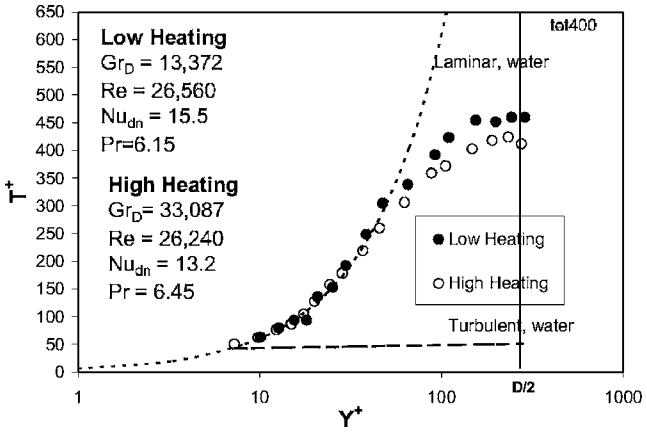

FIG. 2. Effect of Grashof number (i.e., heat flux) on turbulent temperature profiles measured along the vertical plane in the bottom half of the test pipe. Drag-reducing fluid: 400 ppm Ethoquad® plus 300 ppm NaSal in tap water. The drag reduction level for both runs is 73%.

Besides the temperature profile, drag and heat transfer reductions were also measured for each run, at a location 50 mm upstream of the temperature profile measurement. Drag reduction was calculated from the flow velocity and pressure drop measurement, using Eq. (1). Heat transfer reduction was calculated using Eq. (2), while the Nusselt number was evaluated from the measured bulk fluid temperature, heat flux and wall temperature measurements. The wall temperature was measured at three locations on the perimeter of the test tube, bottom, top, and center, to check for buoyancy effects. The calculated Nusselt number (based on the gross parameters) was compared with the Nusselt number calculated from the temperature profile and velocity profile (constructed from the measured drag reduction) and the two were found in good agreement for all reported runs (typically difference less than 3%). For the presentation of the results, a nondimensional temperature and the distance from the wall in the usual wall coordinates were used.[31] The turbulent Prandtl number was then calculated by comparing the slopes of the temperature and velocity profiles.

D. Calibration procedures and accuracy

The two main types of distortions found in the measured temperature profiles were caused by buoyancy and by disturbances of the flow field due to the presence of the temperature sensor. The buoyancy effect is more important in turbulent flows of drag-reducing fluids than in Newtonian flows, due to the reduced convection in the former. To test the buoyancy effects in our experimental installation, one temperature profile was measured at low wall heat flux q''_w (small temperature differences) and another one at high q''_w (under conditions where buoyancy effects could be expected), in both cases keeping the bulk velocity constant. Figure 2 shows the effects of the increase in Grashof number (Gr) on the measured temperature profile, for a 400 ppm cationic surfactant solution (Ethoquad® T13/27 by AKZO-Nobel), which provides slightly less than asymptotic drag reduction in the range of Reynolds numbers covered. For the profile with the low heat flux, the $\Delta T_{w\text{-}b}$ is about 1.6 °C (corresponding to a q''_w=755 W/m^2), whereas for the profile with high heat flux, the $\Delta T_{w\text{-}b}$ was 5.2 °C (corresponding to a q''_w=2100 W/m^2). The temperature profile with the low heat flux does not show a shift of the coldest point (maximum T^+), which is good indicator of the symmetry of the temperature profile. The profile with the high heat flux shows a slight shift of the coldest point towards the bottom wall, however, indicating asymmetry caused by buoyancy. Another consequence of buoyancy is the asymmetry in the radial heat flux. For an average wall-to-bulk temperature difference of about 2 °C, it was estimated, based on the pipe geometry and thermal conductivity, that the radial heat flux (q''_w) would not vary by more than 2% between the top and bottom sides of the pipe. This implies that one could use the constant heat flux approximation for turbulent flow conditions without introducing a significant error. The overall buoyancy effect on the flow asymmetry can be seen from the measurements of Nusselt number. For the two runs shown in Fig. 2, the Nusselt number was calculated from the fluid bulk temperature and the inner wall temperature measured at both top and bottom of the test pipe. For the run at lower heating power, the difference between Nusselt numbers calculated using the top and bottom wall temperature was only 2% (Nu_{up}=15.1, Nu_{dn}=15.5), whereas for the run at higher heating power the difference was 10% (Nu_{up}=12, Nu_{dn}=13.2). A more detailed analysis of the buoyancy in turbulent pipe flows of drag-reducing solutions and its effects on the measurement of temperature profiles can be found in Ref. 37. Our temperature sensor, although small, does affect the flow to some degree, and introduced an error in the measurement; in particular, close to the wall. This effect was reduced by placing the sensor support downstream from the thermocouple bead. In turbulent flows, most of the temperature difference between the wall and the fluid takes place close to the wall, although somewhat less so for drag-reducing than Newtonian flows. This is why an error in the temperature measurements due to disturbance by the sensor is significant. Tests of the sensor are possible only in the viscous sublayer of the turbulent flow or in the laminar flow. For the temperature sensor test, we decided to use a solution of Separan™ polymer with a very high concentration of 1500 ppm, but one which was mechanically degraded before the test. This solution showed somewhat lower drag reduction than asymptotic, and its viscosity was about ten times the viscosity of water at the wall shear stress corresponding to a flow velocity of 1 m/s in our 20 mm test tube. This fluid enabled us to have laminar flow in our test pipe at flow velocities up to 1 m/s.

Figure 3 shows the result of the temperature profile measurements in laminar flow through the test pipe. The temperature difference between the inner wall and the fluid was measured close to the wall in the bottom half of the pipe. Measurements were taken at three levels of heating power: 460, 1750, and 3790 W. For the lowest heating power, 11 measuring points were used, from 0.08 to 1.9 mm from the wall. One can see that above 0.2 mm from the wall, the measurements are in good agreement with the theoretical prediction. The effect of increased heat flux was tested for two locations: 0.78 and 1.88 mm from the wall. The increase in temperature difference is approximately proportional to

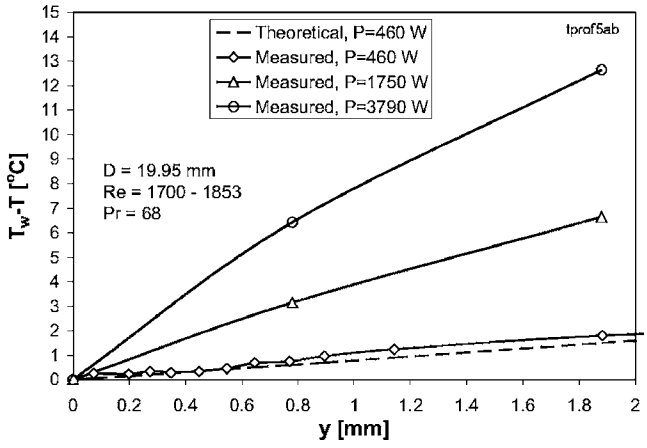

FIG. 3. Test of the temperature sensor in the near-wall region: temperature difference between the wall and the fluid as a function of the distance from the wall. Laminar pipe flow of a drag-reducing surfactant solution (a solution of 1500 ppm of aged Separan™ polymer in water). At the lowest heat flux 11 measuring points were taken, while at the two higher heat fluxes the temperature was measured only at two locations (0.78 and 1.88 mm from the wall). The theoretical temperature profile at the lowest heat flux is shown for the comparison.

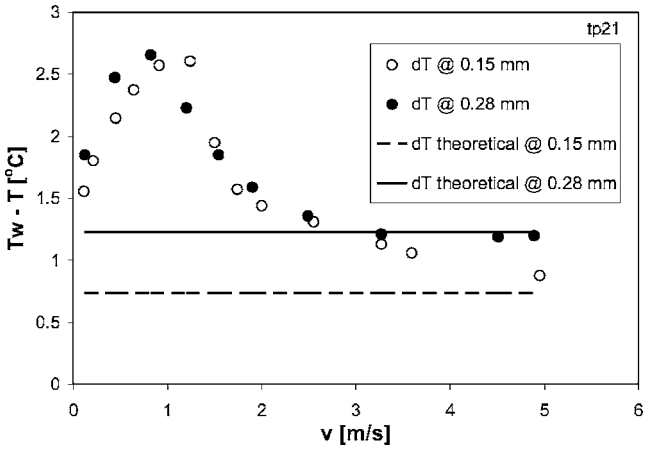

FIG. 4. Difference between the inner wall and fluid temperatures measured at 0.15 and 0.28 mm from the wall, as a function of flow velocity. Drag-reducing solution of 1500 ppm of Separan™ polymer, mechanically degraded by long term circulation. Both locations were inside the viscous sublayer and theoretical values of the temperature difference were calculated for the laminar flow. The wall heat flux was 4000 W/m^2. The peak seen around v=1 m/s seems to be related to the laminar to turbulent transition (Re=2800).

the increase in heating power at 0.78 mm from the wall, but less so at 1.88 mm from the wall. The reason for the deviation at the location further from the wall is likely due to buoyancy effects, which become even stronger toward the pipe center (not shown). As far as disturbance of the flow by the presence of the temperature sensor is concerned, we concluded that our sensor can be used as close as 0.2 mm from the wall, which in most cases corresponds to a y^+ between 5 and 10; i.e., at the edge of the viscous sublayer.

To investigate further the issue of the sensor reliability in the region close to the wall, we performed another test with the same fluid, this time in the critical region between 0.1 and 0.3 mm from the wall and with varying flow velocity. Figure 4 shows the temperature difference between the wall and two locations in the flow field (0.15 and 0.28 mm from the wall) with flow velocities varying between 0.1 and 5 m/s. One can see that the temperature measurements taken at 0.28 mm from the wall are in very good agreement with the theoretical prediction (which is very accurate for the laminar profile deep into the viscous sublayer thickened by the high fluid viscosity) for flow velocities above 3 m/s. The large deviation from the expected result at a velocity of 1 m/s is most likely caused by the laminar to turbulent transition, which is expected exactly at this flow velocity. The measured temperature difference for 0.15 mm from the wall is too high, however, compared with the predicted value. Apparently, the temperature sensor was causing some flattening of the temperature profile when placed too close to the wall, and this should be kept in mind when interpreting the temperature profiles measurements.

As will be shown below for measurements in the turbulent regime, a few measuring points very close to the wall may show a flat temperature profile, a result of fluid mixing caused by the presence of the sensor. In most measurements, however, temperature measurements taken further from the wall coincide with the theoretical laminar temperature profile of the viscous sublayer, as expected. In general, we can say that our measurements can be considered trustworthy starting from the outer edge of the viscous sublayer, or from about $y^+ \approx 8$, for fluids with water-like viscosity, as most of our drag-reducing solutions were.

The uncertainty in the sensor location is primarily affected by the inaccuracy in detecting the wall position ($y=0$), by misalignment of the probe with the direction of the flow, and by the resolution of the micrometer. Note that the error in the sensor position due to misalignment of the probe is a consequence of the L-shaped probe and circular cross section of the channel. The probe was built with an indicator of its direction relative to the direction of the flow, and the uncertainty in direction of the probe was estimated to be about 1°. The overall uncertainty in the sensor location is estimated to be about $1y^+$ or $2y^+$ wall units for most runs.

Altogether, we expect our uncertainty margin for the calculated drag-reduction level (DR) to be about 2% or 3%.[38] This relatively high accuracy is due to the fact that the errors in pipe diameter cancel out in the calculation of DR. The level of uncertainty on the flow velocity is 2% or 3% (mostly due to uncertainty in the inner diameter of the test tube), and considering that the fluids used had mostly water-like viscosity, the uncertainty is about the same for the Reynolds number.

The uncertainty in heat transfer measurements depends strongly on the test conditions (flow rate, heat flux, etc.). By measuring directly temperature differences rather than absolute temperatures, and by applying techniques for electrical noise reduction, we have been able to reduce the uncertainties in the temperature measurements to ±0.05 °C. Despite the efforts taken to improve the accuracy of the temperature measurements, the accuracy of the heat transfer coefficients (Nusselt numbers) could not be improved much beyond 10%, however. This lower limit is imposed by an error of 2% to 3% in the flow rate.[8,38] Somewhat better accuracy is

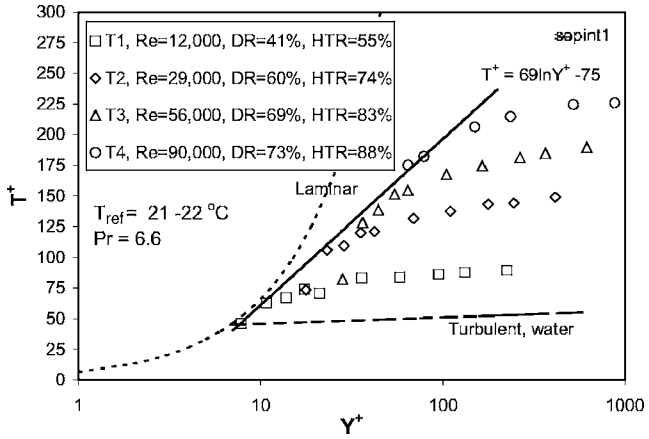

FIG. 5. Temperature profiles measured for a drag-reducing solution of Separan™ polymer. A relatively high concentration of 50 ppm of polymer was needed because the polymer was chemically degraded by aging. Salt (0.5% NaCl) was added to tap water to ensure a coiled conformation of the polymer molecules.

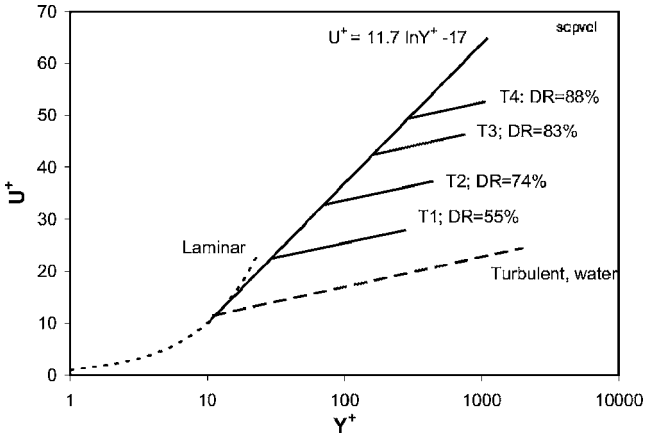

FIG. 6. Velocity profiles corresponding to the measured temperature profiles shown in Fig. 5, calculated from the measured drag reduction using the three-layer model velocity profile for drag-reducing polymer solutions. The buffer layer ($u^+=11.7y^+-17$) grows with increasing level of drag reduction, displacing the turbulent core region.

achieved for the HTR, because some systematic errors—such as the pipe diameter—cancel out. Buoyancy, as a possible source of error during the tests is not included in these figures, but should not be an issue with appropriate limitations on heat flux, as discussed above. Errors in the temperature profile measurements are mostly due to errors in the positioning of the temperature sensors and flow disturbances. Although the tests in laminar flow were satisfactory, some uncertainties do remain for measurements in turbulent flow.

More details on the experimental installation, as well as some measured temperature profiles not reported in this article, can be found in Aguilar.[39]

III. RESULTS AND DISCUSSION

A. Three-layer type profiles

1. Polymers

Figure 5 shows four temperature profiles measured for a 50 ppm solution of Separan™ AP-273 polymer dissolved in tap water with 0.5% of NaCl added to ensure a coiled molecular configuration and therefore type-A drag-reducing behavior.[40] This is a relatively high concentration for this Separan™, which normally provides asymptotic drag reduction at concentrations below 10 ppm. However, our Separan™ sample was about 10 years old and had therefore suffered from chemical degradation, so that the 50 ppm solution showed less than asymptotic drag reduction. For each velocity profile, drag and heat transfer reductions were measured simultaneously with the temperature profiles, and are shown in the graph. At the flow conditions corresponding to all these runs, the shear viscosity at the wall was water-like, and the Prandtl number varied between 6.5 and 6.7 for all the profiles.

All temperature profiles can be approximated as being composed of three distinct layers: a viscous sublayer (for which no measurements were taken, but which certainly exists), a buffer or elastic layer, and a Newtonian-like core. The increase in the HTR associated with increasing velocity is related to an approximately parallel upward shift of the Newtonian-like cores. The thermal sublayer appears not to be significantly thickened compared to the Newtonian profile. The thermal buffer layer (analogous to the momentum buffer layer) for these four profiles seems to be reasonably well represented by a straight line in these semi-logarithmic coordinates, with a slope of approximately 69; i.e., $T^+=69\ln(y^+)-75$ in this case.

Figure 6 presents the estimated velocity profiles corresponding to the temperature profiles presented in Fig. 5. Those velocity profiles were constructed based on drag reduction measurements taken simultaneously with the temperature profiles, and using the Virk's three-layer model as a basis for the velocity profile. Considering that this model has been verified for Separan™ solutions many times by different authors, it is very likely that a velocity profile constructed in this way is as reliable as a direct measurement of the velocity profile, if the drag reduction measurement is accurate. (Figure 11 shows the measured overall friction coefficients corresponding to each of the profiles shown in Figs. 5 and 6, along with measurements using other solutions discussed below. These measurements indicate that the four profiles shown in Fig. 6 were taken well inside the nonasymptotic regime.)

The resemblance of the temperature profiles with the known velocity profiles is obvious. The temperature profiles for polymer solutions exhibiting a typical type-A behavior, such as this Separan™ solution, seem to be well represented by a three-layer model with a buffer layer analogous to that of the velocity profile, and with a Newtonian core region close to the pipe center. This similarity of velocity and temperature profiles suggests a coupling between the diffusivity mechanisms of momentum and heat; i.e., a constant Pr_t.

The Reynolds analogy, which states that the eddy diffusivity for momentum and the eddy diffusivity for heat are identical, results in a similarity of temperature and velocity profiles for flows without pressure gradients. For flow over a plate, with linear velocity and temperature profiles (in the semi-log presentation), the Pr_t can be calculated simply as a ratio of the slopes of the temperature and velocity profiles.

For channel flow, the Reynolds stress and its heat diffusion equivalent are not constant in the radial direction. This means that for an accurate estimate of the Pr_t one has to measure the correlation between flow velocity oscillations in the flow and normal directions for the evaluation of the Reynolds stress, as well as the correlation between temperature and velocity oscillations, as has been done by Li *et al.*[34] For simple developed flows in pipes with a pressure gradient, however, there is reasonable similarity between velocity and temperature profiles, both being close to logarithmic near the wall, even though the similarity of momentum and heat transfer equations is not strictly preserved as is the case with simple external flow over a plate. If one neglects those complexities, one can still calculate the turbulent Prandtl number in pipe flows of Newtonian fluids to be close to 1. This is in agreement with the more rigorously calculated Pr_t in flow of water, which is generally found to deviate no more than 20% from 1, except in the narrow region around $y+=10$, where it likely close to 2 for both flows over a plate and in a pipe.[9]

Based on this analysis, we considered it acceptable to calculate the Pr_t for drag-reducing flows by comparing directly the velocity and temperature profiles, which conveniently turned out to show a constant slope in the buffer region in the semi-log representation. From the slope of our temperature profile estimated at 69 and the slope of Virk's velocity profile being 11.7, we calculate the constant Pr_t for the buffer region to be 6. This is certainly an approximation, having neglected the variation of Reynolds stress and equivalent turbulent heat flux with distance from the wall, but the error is likely not large in relative terms, considering that the Pr_t is so large.

The turbulent Prandtl number for the Newtonian core region is approximately equal to 1, since both temperature and velocity profile slopes are the same as for Newtonian fluids.

We can compare our results with the turbulent Prandtl number calculated by Gupta *et al.*[36] They used direct numerical simulation applying the Peterlin model, which in their previous work on momentum transfer showed a very good agreement with experimental results achieved with polyethylene oxide and other polymers complying with Virk's velocity profile. Although they simulated passive scalar transport in general, they specifically consider the temperature field as their passive scalar, so their results can at least qualitatively be compared to ours. While our turbulent Prandtl number for the asymptotic drag reduction is the same across the whole section of the pipe, they calculated the same numerical value as ours (about 6) for the major part of the outer duct cross section. However, in the region close to the wall their Pr_t sharply increasing with approaching the wall, reaching up to 48. This difference between our and their result may be explained by a possible error introduced in our temperature profile by the presence of the temperature sensor in the region close to the wall, which may have caused mixing and flattening of the temperature profile. A numerical method is certainly advantageous in that respect to any intruding experimental method, at least in qualitative terms. On the other hand, it should be noted that temperature profile calculated by Gupta *et al.*[36] for an asymptotic case at a low Reynolds number showed a heat transfer reduction level which may have been excessively high compared to usually measured values as well as to the value of calculated drag reduction. This would mean that the average turbulent Prandtl number would be too high as well. Despite of this eventuality, the possibility that the turbulent Prandtl number may be higher close to the wall than in the rest of the buffer layer should be given serious consideration.

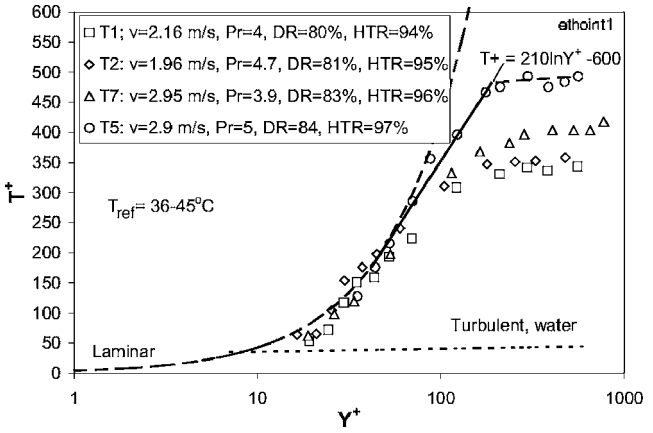

FIG. 7. Temperature profiles measured for a drag-reducing surfactant solution (cationic surfactant Ethoquad® T13/27 at a concentration of 1500 ppm, with 2.5 NaSal/surfactant ratio). No $CuOH_2$ dissolved in tap water. The solution was 1 month old, showing somewhat lover levels of drag reduction than the fresh solution, with the benefit of water-like viscosity.

2. Surfactants

Figure 7 shows temperature profiles measured for a 1500 ppm solution in tap water of the cationic surfactant Ethoquad®, with sodium salicylate added as a counterion in a 2.5 NaSal/surfactant molar ratio. This solution was used in previous tests and was about one month old, with some chemical degradation due to chemical contamination having taken place. We intentionally used this degraded fluid because we have seen that the viscosity of the solution was reduced close to the viscosity of water due to effects of aging (chemical degradation), whereas the drag reduction ability of the fluid, although reduced, remained still high. The viscosity of this fluid was indeed practically the same as that of water at the wall shear stresses achieved in all runs. This is a significant advantage when constructing the nondimensional temperature profile, because the uncertainties in calculating an appropriate shear-dependent viscosity are avoided. The overall friction coefficient measurements corresponding to each of these profiles are listed in Fig. 11, showing high—but less than asymptotic—levels of drag reduction.

The temperature profiles for this surfactant solution show the following distinctive characteristics. (1) A thickened thermal sublayer up to at least a y^+ of 20 or 30, in contrast to the Separan™ polymer solution, which showed an unaffected sublayer (compared to the Newtonian case) extending only to $y^+ \approx 10$. (2) The slope of the buffer layer of all these profiles is about three times larger than the slope measured for the polymer solutions. In terms of wall coordinates, an average thermal buffer layer for all these profiles

can be expressed as $T^+=210\ln(y^+)-600$. (3) All profiles show a remaining logarithmic core layer, displaced approximately parallel to the Newtonian layer, even the profile T5, which is very close to asymptotic. Note that all four runs were conducted at relatively high fluid temperature, the reference temperature (the average between bulk and wall temperatures) being between 36 and 45 °C. The run with the highest temperature (45 °C) is the one with temperature profile labeled T7. This surfactant solution started to show signs of temporary thermal degradation. This is likely the reason why the drag reduction for T7 (Fig. 11) is not increasing relative to T5 despite an increased Reynolds number, the temperature profile T7 lying in fact below T5.

We may now compare these temperature profile characteristics to some of the velocity profiles measured for cationic surfactants in the past, in order to determine whether a similarity between velocity and temperature profiles can be established for drag-reducing cationic surfactant solutions. The first characteristic of our temperature profiles—the thickened thermal sublayer—does not seem to agree with the surfactant velocity profiles of Povkh *et al.*,[22] who claimed that the viscous sublayer remained the same as for Newtonian fluids. This characteristic does not agree with the velocity profiles presented in Ref. 23 for a (tetradecyltrimethylammonium bromide) TTAB+NaSal solution, which shows an unaffected viscous sublayer followed by a buffer layer extending all the way to the pipe center. The difficulty with both of those velocity profiles is that their buffer layer, which started at $y^+=5$, crosses the theoretical viscous sublayer at both $y^+=5$ and $y^+=30$. This means that within that region (which they consider to be the buffer layer) there is even a lower diffusivity than a purely molecular diffusion process (i.e., a laminar profile) would have, which appears physically impossible. Since the authors have used a constant viscosity (at low shear rates) for the determination of y^+, a possible explanation for their conclusion is that they have overestimated the actual shear viscosity and thus obtained a profile that is shifted towards the y^+ axis.

The second characteristic we noted—the slope of the buffer layer—is qualitatively in good agreement with the increased slope of asymptotic velocity profiles for surfactant solutions, e.g., as in Ref. 27, where proposed slope of the velocity buffer layer for surfactants is 23.4 (instead of 11.7 for polymer solutions). In fact, it is because of this increased slope that the increment in the sublayer thickness becomes almost a necessary requirement. Otherwise, it would have to be accepted that the gradient of the profile is at some point larger than that for a fully laminar profile.

Finally, the turbulent Newtonian-like logarithmic core seems to show up in velocity profiles of various surfactant systems as well. Results by Bewersdorff and Ohlendorf[16] and Chara *et al.*[25] consistently show that—unlike most polymer solutions—this Newtonian-like logarithmic layer is always present in the velocity profiles of surfactants, even at what they considered to be asymptotic conditions.

Figure 8 shows the calculated velocity profiles corresponding to the four temperature profiles shown in Fig. 7. The calculations are based on the level of drag reduction measured simultaneously with each temperature profile, and

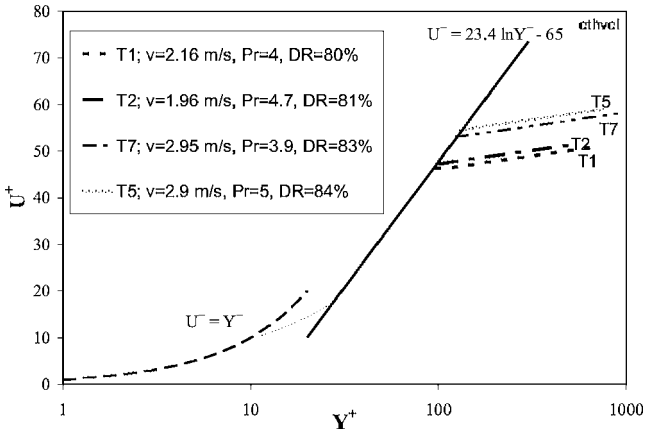

FIG. 8. Velocity profiles corresponding to the measured temperature profiles shown in Fig. 7, calculated from the measured drag reduction using the three-layer model for velocity profile. The buffer layer ($u^+=23.4y^+-65$), proposed by Chara *et al.* (Ref. 25) for surfactant solutions, grows with increasing level of drag reduction, displacing the turbulent core region.

the assumption that the elastic layer for surfactant solutions has a slope of 23.4 in the semi-log coordinates, as proposed by Zakin *et al.*[27] (We used a transition region between the viscous sublayer and buffer layer for integration.) If one accepts this three-layer profile for velocity, there appears to be similarity between temperature and velocity profiles, just as it is the case with polymer solutions. The turbulent Prandtl number calculated as a ratio between the slopes of the temperature and the velocity profiles is calculated to be 9. This value can be assigned up to the y^+ at the end of the elastic layer, i.e., 150. The match between the temperature and velocity profiles beyond that point is hard to ascertain because of inaccuracies of the procedure. In any case, the region towards the center of the pipe appears to have much less effect on the friction and heat transfer than the region closer to the wall.

It is interesting to compare our result with the result for Pr_t found by Li *et al.*[34] Li *et al.* calculated Pr_t for the cationic surfactant solution by measuring the velocity and temperature profiles, as well as the Reynolds stress and turbulent heat transfer normal to the wall. Their results were very different from ours. For one of their three runs, the one with the highest level of drag reduction, their calculated Pr_t was highest at $y^+=13$, with a value of about 18, falling to about 1 at $y^+=60$, and remaining at somewhat below 1 (as for water) for the rest of the measured profile up to $y^+=350$. One noteworthy issue is that the temperature and velocity profiles measured by Li *et al.* are very dissimilar from each other. On the one hand, their velocity profile above the sublayer has a constant slope—increased relative to the Newtonian profile, but lower than Virk's asymptotic profile—and reaching to the very center of the pipe. On the other hand, the slope of their temperature profile in most of the measured region was practically the same as for water. The whole upward shift relative to water in their temperature profile appeared to take place in the region of y^+ between 10 and 25. The main reason for the difference between the results for turbulent Prandtl number by Li *et al.* and our results, is likely not our assumption of

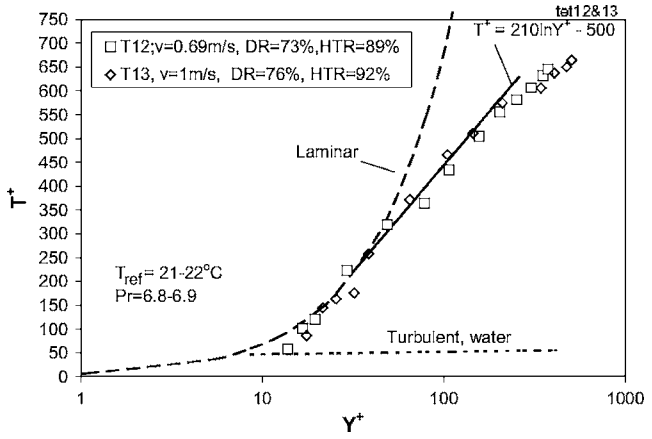

FIG. 9. Asymptotic temperature profiles measured for a fresh solution of Ethoquad® T13/27 surfactant. This solution contained 1500 ppm of the surfactant with a 0.6 NaSal/surfactant molar ratio, and also 0.5 mM/l of $Cu(OH)_2$, dissolved in tap water. Asymptotic levels of drag and heat transfer reductions were measured simultaneously with the temperature profiles.

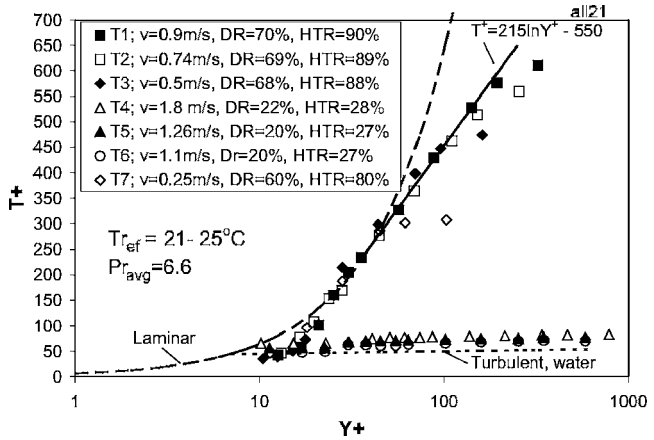

FIG. 10. Temperature profiles measured for a weak surfactant solution. The solution used for these measurements was the same solution of Ethoquad® used for the measurements of the temperature profiles shown in Fig. 9, but 3 months old.

constant eddy diffusivities of momentum and heat with y^+, but rather the dramatic difference between their and our temperature profiles. While our temperature profiles were similar to the known velocity profiles, with the slope being six times higher than the slope of the velocity profile in the whole region above the sublayer, the slope of their temperature profile was about four times lower than the slope of their velocity profile for y^+ above 25. It is very hard to explain this large difference between the temperature profiles measured by Li *et al.* and ourselves. One can only conclude that more temperature profile measurements are needed over a wide range of drag-reducing solutions and flow conditions.

Note that a thickening of the viscous sublayer relative to the Newtonian case—if present to the same extent in both velocity and temperature profiles—would cause higher levels of heat transfer reduction than drag reduction, even at a turbulent Prandtl number equal to 1, for fluids with a molecular Prandtl number higher than 1 (as for water which has a Pr of about 7 at 20 °C). Indeed, many researchers who measured velocity profiles of drag-reducing fluids reported a sublayer thickening.[41] The issue of the thickening of the viscous sublayer is still somewhat elusive, because of problems associated with measurements close to the wall. As we have seen in the temperature profile for Ethoquad® (and similarly in the velocity profile), an apparent sublayer thickening appears inevitable for the larger slopes of the buffer layer pertaining to surfactant solutions. This thickening would have to be very large to account for the measured difference in the overall heat transfer and drag reductions, however, if the slopes of velocity and temperature profiles out of the sublayer were the same.

a. Effect of $Cu(OH)_2$ *and aging on cationic surfactant solution.* We have seen that the presence of copper ions in cationic surfactant solutions has strong effects on their drag-reducing properties. The addition of copper hydroxide $Cu(OH)_2$ reduces the viscosity of solutions of Ethoquad®, as well as its drag-reducing ability at lower Reynolds numbers, but increases its resistance to mechanical degradation and its drag reduction at high Reynolds numbers. With aging, cationic surfactant solutions generally see a decrease in their drag-reducing ability.

We measured the temperature profile of a freshly prepared solution of Ethoquad® T13/27 at a surfactant concentration of 1560 ppm, plus sodium salicylate as counter-ion in a 0.6 NaSal-to-surfactant molar ratio, and with an added 0.5 mM/l of $Cu(OH)_2$. The viscosity of this solution was essentially the same as for water, and any variations in Prandtl number were due to variations in temperature. After we used the same solution for 3 months of testing mechanical degradation and recovery, we measured the temperature profiles again, and saw that the solution became weak; i.e., it was easily degraded. About 100 s were also necessary for the drag and heat-reducing effects to develop fully in the pipe after the start of the flow, at a flow velocity of 0.6 m/s. This long time is attributed to slower development of micellar structures or shear-induced state.

Figure 9 shows temperature profile measurements at two flow velocities, i.e., 0.6 and 1 m/s, for the freshly prepared fluid with $Cu(OH)_2$. Global measurements of HTR for both flow velocities (as well as those calculated by integrating temperature profiles) showed asymptotic values, as was the case with measured drag reduction (Fig. 11) as well. One interesting aspect of the temperature profiles shown in Fig. 9 is that the whole cross section of the flow is affected by the HTR effects; i.e., there is no noticeable turbulent core region up to the last datum, which is close to the center of the pipe. This suggests that the Newtonian-like core region that was measured in most cases of asymptotic velocity and temperature profiles for surfactant solutions, but which did not typically appear in asymptotic profiles of polymer solutions and is also missing here, may not necessarily imply any essential difference between polymer and surfactant drag-reducing solutions. The slope of the logarithmic temperature profile in the elastic layer is about 210, basically the same as for Ethoquad® solution without addition of copper hydroxide. The type of profile is different from that seen in Fig. 7 for the same surfactant without the $Cu(OH)_2$, however.

Figure 10 shows similar measurements about 3 months

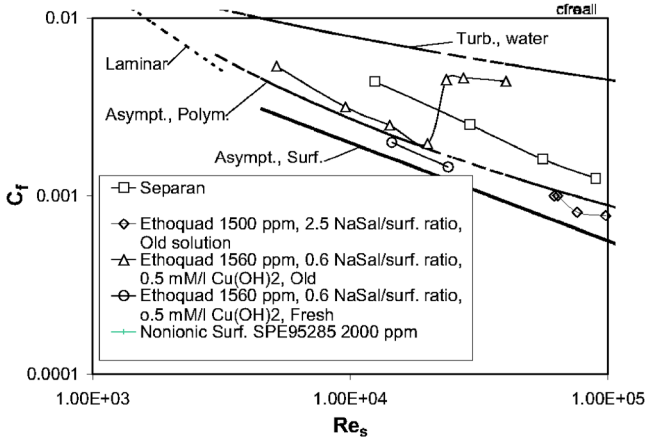

FIG. 11. Drag-reduction characteristics (C_f vs Re) for various drag-reducing solutions used for our temperature profile measurements. All the measurements were conducted in a test pipe tube with an inner diameter of 19.95 mm, at a location more than 500 diameters from the tube entry.

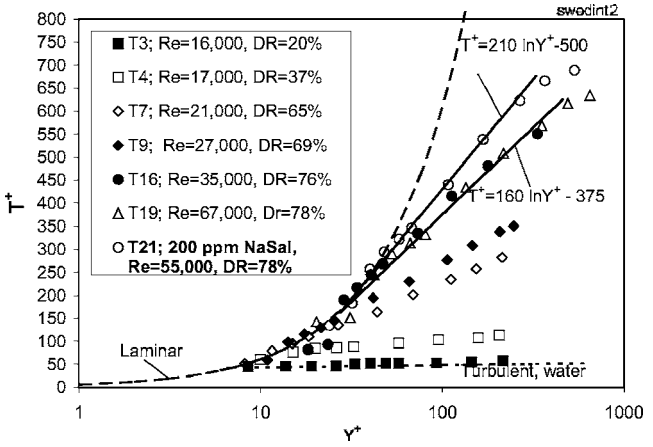

FIG. 12. Temperature profiles for a water-based solution of the nonionic surfactant SPE 95285. All profiles, except T21, were measured for a solution with surfactant concentration of 2000 ppm dissolved in tap water. For profile T21, 200 ppm of sodium salicylate was added to the surfactant solution used for the other runs. The molecular Prandtl number varied between 5.5 and 6.5. The runs corresponding to temperature profiles T16, T19, and T21 showed asymptotic levels of drag reduction.

later, using the same fluid. For flow velocities up to 0.9 m/s, the global HTR measurements as well as overall drag reduction measurements (Fig. 11) show somewhat lower than asymptotic values, but the temperature profiles include one datum, possibly suggesting a small turbulent core region. For velocities higher than 0.9 m/s the degradation in the test tube during the run is obvious. The heat transfer reduction decreases with increasing flow velocity with a displacement of the temperature profile towards lower values of T^+ and closer to the profile of water. The slope of the elastic layer is 215, again basically the same as for all other Ethoquad® solutions.

B. Fan-type profiles

We now turn to the measurements of temperature profiles for drag-reducing solutions for which velocity profiles are not well established. Figure 12 shows nonasymptotic temperature profiles for a solution of a custom biodegradable nonionic surfactant (SPE 95285 by AKZO-Nobel) diluted in tap water. The nominal surfactant concentration was 2000 ppm, plus 500 ppm initial concentration of biocide (Nalco 2810). The changes in the profiles due to an increase in velocity show a very distinctive behavior in comparison to those of the cationic surfactant solutions seen before. Each of these profiles corresponds to different levels of HTR, but rather than having one single region close to the wall where most of the drag and heat transfer reduction effects take place (i.e., a buffer layer as in the classic three-layer profiles), the heat transfer reduction effects are seen all the way to the center, even at low levels of reduction. This is what we refer to as a "fan-type" behavior.[35] Higher levels of HTR are achieved here by increasing the slope of the temperature profile rather than by increasing the thickness of the buffer layer. (Note that for all these profiles, the pipe center is only between 25 and 75 wall units away from the last datum point). Even at low levels of reduction, no significant Newtonian logarithmic layer is seen (the pipe center in terms of y^+ varies for each profile).

Hoyer and Gyr[15] reported a similar fan-type pattern of velocity profiles for heterogeneous drag reduction (where a highly concentrated streak of polymer is ejected in the pipe core). They concluded that such a velocity profile pattern was associated with "an entanglement of multiple polymer molecules capable of affecting the entire pipe diameter even at low drag reduction levels." For both types of fluids, i.e., homogeneous and heterogeneous solutions, it seems likely that a critical shear stress or turbulence dynamics would play a role, although additional factors like stress history may complicate the picture in a different way for the two kinds of drag-reducing fluids.

Another implication may be related to scaling correlations.[35] We have shown that a 4000 ppm solution of the same SPE 95285 surfactant did not follow the scaling correlation based on DR versus flow velocity—which most polymers and the cationic surfactant solution complied with—but rather an alternative one given by τ_w versus velocity, as also proposed by Schmitt *et al.*,[42] supposedly for all surfactant solutions. An analysis of the differences between these two correlations was undertaken by Aguilar.[39] It was shown for friction that the difference between the two scaling procedures had to be related to either a variation in the onset of drag reduction (i.e., a different wall shear stress at the onset) for different pipe diameters and/or a variation in the slope of each of the friction coefficient curves for the different diameters. It was further shown that fluids exhibiting a ΔB^+-type profiles do scale according to the DR versus velocity correlation, and those fluids exhibiting a fan-type velocity profile scaled according to the τ_w versus velocity correlation. Interestingly, the velocity profile measurements carried out by Bewersdorff and Ohlendorf[16] for CTAB surfactant solutions showed an apparent fan-type velocity profile analogous to the fan-type temperature profiles that we measured for the same fluid that Schmitt *et al.*[42] used to show the validity of the τ_w versus velocity scaling procedure. This finding does strengthen our conclusion of a relationship

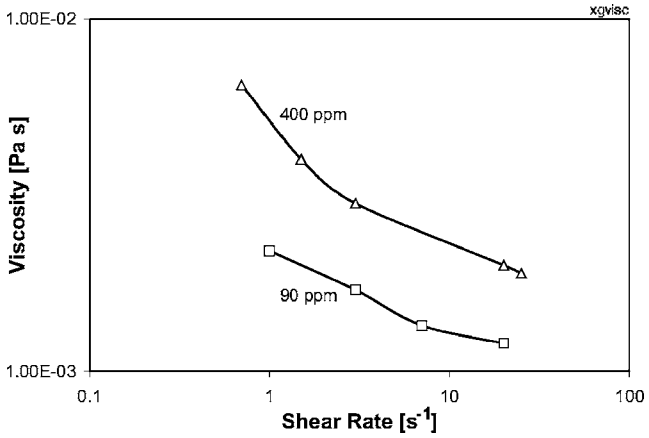

FIG. 13. Viscosity of Xanthan gum at concentrations of 400 and 90 ppm. The measurements were taken in capillary tubes of inner diameters 0.723 and 2 mm.

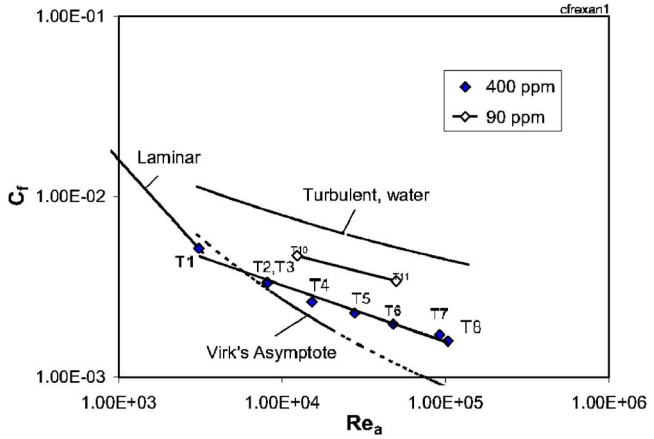

FIG. 14. Drag-reducing characteristics of the 90 and 400 ppm Xanthan gum solutions in deionized water. Drag reduction is constant with respect to the Reynolds number, as is typical for type-B drag-reducing solutions, except for run T1, for which the level of drag reduction was limited by the asymptote.

between ΔB^+-type profiles with the DR versus velocity scaling correlation, versus—on the other hand—fan-type profiles with the τ_w versus velocity scaling correlation.

C. Type-B drag reducer (Xanthan gum)

Virk and Wagger[40] introduced the concept of type-B drag reduction. This type of drag reduction is exhibited by stretched and rigid polymer molecules, contrary to the coiled polymer molecules that exhibit type-A drag reduction. Some polymers may show both type-A and type-B drag reduction depending on the salt content in the solution, the salt facilitating coiling of the molecules. The difference in drag reduction characteristics between a type-A and a type-B drag reducer in the C_f-Re presentation is that drag reduction of a type-A solution increases with increasing Re, starting from the onset point at which wall shear stress becomes large enough to cause stretching the molecules, whereas a type-B solution shows asymptotic drag reduction immediately after the transition from laminar to turbulent flow. The retro-onset point for a type-B drag reducer is the point at which drag reduction stops increasing with increasing Re, with the drag reduction remaining constant with further increases of Re until mechanical degradation occurs.

For type-B drag-reducing fluids, the variations of velocity profiles with increasing flow velocity are not known. To investigate this issue, we measured temperature profiles of a type-B drag-reducing solution, taking advantage of a likely similarity between velocity and temperature profiles as was demonstrated for type-A solutions of Separan™ polymer and Ethoquad® surfactant. Two solutions of a typical type-B Xanthan gum drag-reducing polymer were prepared in deionized water, at concentrations of 90 and 400 ppm. Studies of the drag-reducing characteristics of Xanthan gum showed that this is indeed a good example of a type-B fluid.[43] Because of the relatively low molecular weight of Xanthan gum, the solution viscosity is necessarily higher than water viscosity if significant levels of drag reduction are to be achieved. Figure 13 shows results of shear viscosity measurements for both Xanthan gum solutions used in our tests, as measured in capillary tubes with diameters of 0.723 and 2 mm. As one can see, in the range of shear rates between 1 and 20 s^{-1}—which is the range applicable to our tests—the viscosity of both solutions is several times higher than the viscosity of water and this will have to be considered in the nondimensionalization of the temperature profiles. Figure 14 shows drag reduction measurements for all runs in which the temperature profiles were measured, for both 90 and 400 ppm solutions. The constancy of DR at high Reynolds numbers is clearly seen.

Figure 15 shows a series of temperature profiles corresponding to various Reynolds and Prandtl numbers for the 400 ppm solution. The Prandtl numbers corresponding to each profile are computed based on an apparent viscosity at the wall calculated from laminar data. The Newtonian laminar profiles corresponding to Pr=15, 22, and 33 are plotted as reference. The Prandtl numbers are given for each run, depending on the wall shear stress for that particular run. The

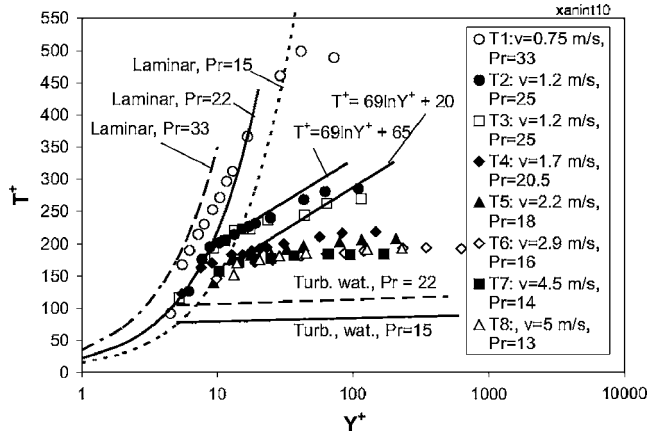

FIG. 15. Temperature profiles measured for a 400 ppm solution of Xanthan gum in deionized water. Constant levels of drag and heat transfer reductions were measured for all runs (DR=60%, HTR=70%), except for run T1 at the lowest flow velocity, for which the reductions were limited by the asymptotes (DR=52%, HTR=55%). The thermal buffer layers found as best fit for the temperature profiles of the Separan™ polymer solution ($T^+=69 \ln y^+ + C^t$) are shown for comparison.

viscosity corresponding to the wall shear stress was used for the calculation of the nondimensional temperature profile regardless of the nondimensional distance from the wall y^+, despite shear-thinning effects. Drag and heat transfer reductions were the same for all runs (DR=60%, HTR=70%), except for the run at the lowest velocity (T1), for which DR was 51% and HTR was 55%. For run T1 the measured temperature profile was close to the laminar profile at the same Prandtl number of 33. As the flow velocity increases, the temperature profiles get closer to the temperature profile of water, a necessary requirement to maintain a constant level of heat transfer reduction. For all temperature profiles except T1, a thickening of the viscous sublayer appears to be the dominant feature of the profiles corresponding to heat transfer reduction. For instance, for profile T8 (that with the lowest Prandtl number, i.e., the highest flow velocity), a thickening of the sublayer to $y^+ \approx 12$ is observed, whereas for profiles T2 and T3 (those with the highest Prandtl number and lowest velocity after T1) ,the sublayer reaches a thickness of about 10 wall units ($y^+ \approx 10$). According to well-established heat transfer correlations, the corresponding sublayer thicknesses for Newtonian fluids with similar Prandtl number as those of profiles T8 and T9 are about 6 and 4 (in y^+ units), respectively. This means that the sublayer in both cases was thickened between 2 and 3 times compared to a Newtonian fluid, significantly more than for the type-A drag-reducing polymers.

Considering asymptotic runs such as T2 and T3, we would expect for a type-A polymer solution that the elastic layer would be linear and would extend to the center of the pipe. (An elastic layer with a slope of 69 in semi-log coordinates—as found for our type-A drag-reducing polymer Separan™—is shown for reference in Fig. 15). Instead, we see that the increase of the nondimensional temperatures caused by the apparent thickening of the sublayer is negated by a reduced slope towards the center of the tube. (This is because T_b^+—the temperature at the location corresponding to the bulk velocity—is known for a given level of heat transfer reduction at a given velocity.) The effect of the increased flow velocity is seen as a lowering of the logarithmic temperature profile, as is necessary to maintain the constant level of drag and heat transfer reductions seen in this type-B solution (Fig. 14).

Outside of the sublayer, compared to the type-A profile one could interpret the overall lowered type-B profile as being either a lowered slope elastic layer extending to the center, or alternatively as an elastic layer of similar slope followed by a Newtonian core in the outer region. The data are ambiguous in this respect.

One can attempt to explain this apparent difference between the temperature profiles for type-A and type-B surfactant solutions by a different effect of the elongated molecules (characteristic of the type-B behavior) versus coiled ones (characteristic of the type-A fluids). However, considering that the difference in temperature profiles for type-A and type-B polymer solution is not so large, one may also consider the effect of the significantly increased viscosity of the Xanthan gum solution relative to the viscosity of the Separan™ solution. Significant sublayer thickening have also been observed by some researchers through the measurement of velocity profiles for surfactant solutions, and this thickening has usually been attributed to an increased shear viscosity—which is generally much larger in the case of surfactant solutions than in high molecular weight polymer solutions (typically 4 times or more). Some ambiguity in defining the relevant apparent viscosity as that corresponding to the wall shear stress, as well as neglecting the variation of viscosity as function of the distance of the wall, certainly do introduce some uncertainty in evaluating the nondimensional temperature profile of solutions with increased shear-dependent viscosity. The reference model of the temperature profile of Newtonian fluids used in our graphs is certainly a crude—although generally used—approximation, based on the artificial distinction of the purely viscous and turbulent regions in the flow.

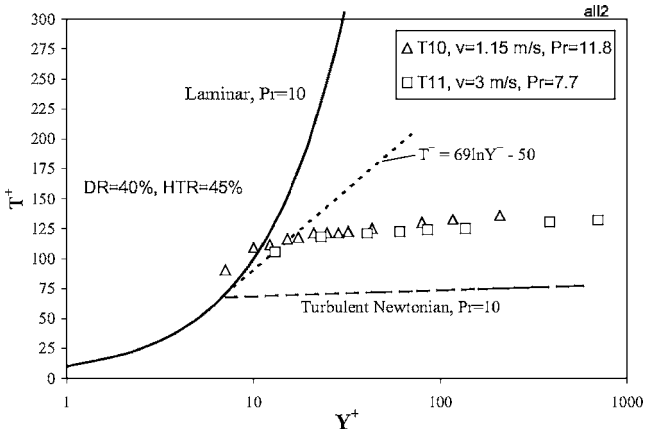

FIG. 16. Temperature profiles measured for a 90 ppm solution of Xanthan gum in deionized water. The viscosity of this solution is much closer to the viscosity of water and much less shear-dependent than the viscosity of the 400 ppm solution. The thermal buffer layer found as best fit for the temperature profiles of Separan™ polymer solution ($T^+=69 \ln y^+ + C$) is shown for comparison.

We have also tested the solution of Xanthan gum with a lower concentration of 90 ppm in order to reduce the effect of increased viscosity. Unfortunately, the level of drag and heat transfer reductions for those runs were only 40% and 45%, respectively, which is much lower than for the runs with the 400 ppm solution. Some temperature profiles for those runs are presented in Fig. 16. For profile T11 at a flow velocity of 3 m/s, the Prandtl number is 7.7 and the viscosity is only slightly higher than for water. An elastic layer with a slope of 69, as found for the type-A Separan™ solution, is shown for reference. The low level of heat transfer reduction does not, however, allow us to differentiate between a thickening of the sublayer and a thin elastic layer profile of type-A slope followed by a Newtonian core layer. For the temperature profile T10, measured at a velocity of 1.15 m/s, the measured points close to the wall penetrate inside the viscous sublayer, indicating problems with the temperature measurements close to the wall, as expected for fluids with increased viscosity.

Altogether, the difficulties resulting from the increased viscosity of this solution prevents us from obtaining more definitive conclusions about the nature of the profiles for this

type-B fluid, besides shifting of the drag reduction effects towards the wall, such as an apparent thickening of the sublayer.

IV. SUMMARY AND CONCLUSIONS

Measurements of temperature profiles for a polymer solution showed that the temperature profiles were similar to Virk's three-layer velocity profile, with a thermal buffer layer analogous to the velocity buffer layer. A temperature model analogous to the three-layer velocity model offers a good description of how the HTR level increases with increasing Reynolds number. The appearance and increase in HTR is related to the appearance and growth of a thermal buffer layer (of slope 69 in the semi-logarithmic coordinates) which causes a displacement of the Newtonian logarithmic layer. This latter layer is progressively shortened until it practically disappears when asymptotic HTR is reached.

Similar profiles are seen for a cationic surfactant solution (Ethoquad® T13/27), except that in this case the thermal sublayer is thickened by a factor of 2 to 3 relative to the Newtonian case, whereas it remains essentially unaffected for the Separan™ solution. The thermal buffer layer slope of 210 in the semi-logarithmic coordinates is three times larger for this surfactant solution than for the polymer solution. This increased slope of the temperature profile can be seen as a reason for the apparent thickening of the sublayer. Even for asymptotic temperature profiles, a relatively unaffected region far away from the wall (a remaining Newtonian-like logarithmic layer) is still observed. Altogether, the characteristics of the drag and heat transfer reduction phenomena for this group of fluids (polymer and surfactant solutions) do match well with the classic model where apparent drag reduction effects take place within a buffer (elastic) layer.

In general, temperature profiles are analogous to the velocity profiles which are well documented for those fluids, resulting in an estimated Pr_t of about 6 for a polymeric solution and 9 for a surfactant solution. The supported assumption of a constant Pr_t allows us then to use temperature profile measurements for other fluids—for which we do not know the velocity profiles—as a tool for the general analysis of drag reduction phenomenology.

Aging and contamination with chemicals, particularly copper compounds, do strongly affect drag-reducing properties of cationic surfactant solutions. A fresh solution of Ethoquad® surfactant treated with copper hydroxide showed a continuous linear temperature profile practically to the center of the pipe, and without significant Newtonian core. Three months old solutions showed the same linear slope for the temperature in the elastic layer, but with a Newtonian-like core.

The temperature profiles of a nonionic surfactant solution (SPE 95285) showed a pattern very different from all previously measured temperature profiles. These profiles show a fan-type pattern. Even at low levels of heat transfer reduction, the whole profile stretching from the wall to the pipe center is changed relative to the Newtonian profile, with no remaining Newtonian-like core region. Consequently, there are no distinctive elastic and core regions as in the Virk's model. Instead of a thickening of the elastic layer, the slope of the linear temperature profile (in the usual semi-log coordinates) is increasing with increasing levels of heat transfer reduction.

Temperature profiles measured for the type-B drag-reducing polymer Xanthan gum showed some differences with the profiles measured for the type-A drag-reducing polymer Separan™. The asymptotic profile for a 400 ppm solution of Xanthan gum showed a thickening of the sublayer and a somewhat smaller slope further from the wall, compared to temperature profiles for Separan™. The difference, however, was small and may be attributed to the effects of increased and shear-dependent viscosity of that solution.

ACKNOWLEDGMENTS

We acknowledge gratefully the financial support of the California Energy Commission (Contract No. 500-94-022 to E.F.M.—D. Hatfield, Program Manager) and the generous supply of surfactants by Dr. S. Shapiro and Dr. M. Hellsten (AKZO-Nobel Chemicals). G.A. also wishes to acknowledge the *Universidad Nacional Autonoma de Mexico*, and especially the DGAPA and the IIM for support granted through their scholarship program. Thanks are also due to Dr. K. Hoyer for very useful discussions on drag reduction.

[1] P. S. Virk, H. S. Mickley, and K. A. Smith, "The ultimate asymptote and mean flow structure in Toms' phenomenon," J. Appl. Mech. **37**, 488 (1970).
[2] P. K. Ptasinski, B. J. Boersma, F. T. M. Nieuwstadt, M. A. Hulsen, B. H. A. A. Van den Brule, and J. C. R. Hunt, "Turbulent channel flow near maximum drag reduction: Experiments and mechanisms," J. Fluid Mech. **490**, 251 (2003).
[3] Y. E. M. Khabakpasheva and B. V. Perepelitsa, "Turbulent heat transfer in weak polymeric solutions," Heat Transfer-Sov. Res. **5**, 117 (1973).
[4] B. Yu and Y. Kawaguchi, "Parametric study of surfactant-induced drag-reduction by DNS," Int. J. Heat Fluid Flow **27**, 887 (2006).
[5] J. L. Lumley, "Drag reduction by additives," Annu. Rev. Fluid Mech. **1**, 367 (1969).
[6] P. G. De Gennes, "Towards a scaling theory of drag reduction," Physica A **140**, 9 (1986).
[7] K. Gasljevic and E. F. Matthys, "Improved quantification of the drag reduction phenomenon through turbulence reduction parameters," J. Non-Newtonian Fluid Mech. **84**, 123 (1999).
[8] G. Aguilar, K. Gasljevic, and E. F. Matthys, "Coupling between heat and momentum transfer mechanisms for drag-reducing polymer and surfactant solutions," J. Heat Transfer **121**, 796 (1999).
[9] W. M. Kays, "Turbulent Prandtl number—where are we?," J. Heat Transfer **116**, 284 (1994).
[10] Y. I. Cho and J. P. Hartnett, "Non-Newtonian fluids in circular pipe flow," Adv. Heat Transfer **15**, 59 (1982).
[11] K. Gasljevic and E. F. Matthys, "Experimental investigation of thermal and hydrodynamic development regions for drag-reducing surfactant solutions," Trans. ASME, J. Appl. Mech. **119**, 80 (1997).
[12] T. Mizushina and H. Usui, "Reduction of eddy diffusion for momentum and heat in viscoelastic fluid flow in a circular tube," Phys. Fluids **20**, S100 (1977).
[13] H. K. Yoon and A. J. Ghajar, "A new heat eddy diffusivity equation for calculation of heat transfer to drag-reducing turbulent pipe flows," *Proc. of the Eighth International Heat Transfer Conference*, San Francisco, edited by C. L. Tien, U. P. Carey, and J. K. Ferrell (Hemisphere, Washington, DC, 1986), pp. 937–942.
[14] T. R. Roethig and E. F. Matthys, "Eddy diffusivities for non-isothermal tube flow of drag-reducing polymer solutions," in *Proceedings of the 10th International Congress on Rheology*, edited by P. Uhlherr (Australian Soc. Of Rheology, Sydney, 1988), Vol. 2, pp. 227–229.
[15] K. Hoyer and A. Gyr, "Turbulent velocity field in heterogeneously drag reduced pipe flow," J. Non-Newtonian Fluid Mech. **65**, 221 (1996).

[16]H. W. Bewersdorff and D. Ohlendorf, "The behavior of drag-reducing cationic surfactant solutions," Colloid Polym. Sci. **266**, 941 (1988).
[17]A. Rollin and F. A. Seyer, "Velocity measurements in turbulent flow of viscoelastic solutions," Can. J. Chem. Eng. **50**, 714 (1972).
[18]T. T. Huang, "Similarity laws for turbulent flow of dilute solutions of drag-reducing polymers," Phys. Fluids **17**, 298–309 (1974).
[19]M. M. Reischman and W. G. Tiederman, "Laser-Doppler anemometer measurements in drag-reducing channel flows," J. Fluid Mech. **70**, 369 (1975).
[20]T. Q. Li and K. L. McCarthy, "Pipe flow of aqueous polyacrylamide solutions studied by means of nuclear magnetic resonance imaging," J. Non-Newtonian Fluid Mech. **57**, 155 (1995).
[21]M. P. Escudier, F. Presti, and S. Smith, "Drag reduction in turbulent pipe flow of polymers," J. Non-Newtonian Fluid Mech. **81**, 197 (1999).
[22]I. L. Povkh, A. V. Stupin, and P. V. Aslanov, "Structure of turbulence in flows with surfactant and polymeric additives," Fluid Mech.-Sov. Res. **17**, 65 (1988).
[23]A. Gyr and H. W. Bewersdorff, *Drag Reduction of Turbulent Flows by Additives* (Kluwer, Dordrecht, 1995), pp. 162–163.
[24]H. W. Bewersdorff, "Drag reduction in surfactant solutions," in *Structure of Turbulence and Drag Reduction*, edited by A. Gyr (Springer, Berlin, 1990), pp. 293–312.
[25]Z. Chara, J. L Zakin, M. Severs, and J. Myska, "Turbulence measurements of drag-reducing surfactant systems," Exp. Fluids **16**, 36 (1993).
[26]H. W. Bewersdorff and N. S. Berman, "The influence of flow-induced non-Newtonian properties on turbulent drag reduction," Rheol. Acta **27**, 130 (1988).
[27]J. L. Zakin, J. Myska, and Z. Chara, "New limiting drag reduction and velocity profile asymptotes for non-polymeric additives systems," AIChE J. **42**, 3544 (1996).
[28]G. Aguilar, K. Gasljevic, and E. F. Matthys, "Asymptotes of maximum friction and heat transfer reductions for drag-reducing surfactant solutions," Int. J. Heat Mass Transfer **44**, 2835 (2001).
[29]B. F. Blackwell, W. M. Kays, and R. J. Moffat, Report HMT-5, Thermosciences Division, Department of Mechanical Engineering, Stanford University, 1972.
[30]D. K. Hollingsworth, W. M. Kays, and R. J. Moffat, Report HMT-41, Thermosciences Division, Department of Mechanical Engineering, Stanford University, 1989.
[31]W. M. Kays and M. E. Crawford, *Convective Heat and Mass Transfer*, 3rd ed. (McGraw-Hill, New York, 1993).
[32]C.-F. Li, R. Sureshkumar, and B. Khomami, "Influence of rheological parameters on polymer induced turbulent drag reduction," J. Non-Newtonian Fluid Mech. **140**, 23 (2006).
[33]Y. Kawaguchi, H. Daisaka, A. Yabe, K. Hishida, and M. Maeda, "Existence of double diffusivity layers and heat transfer characteristics in drag-reducing channel flow," in *Turbulence, Heat and Mass Transfer 2: Proc. of the 2nd Int. Symp.*, Delft, June 9–12, 1997, edited by K. Hanjalic and T. W. Peters (Coronet Books, Philadelphia, 1997).
[34]F.-C. Li, Y. Kawaguchi, and K. Hishida, "Investigation on the characteristics of turbulence transport for momentum and heat in a drag-reducing surfactant solution flow," Phys. Fluids **16**, 3281 (2004).
[35]K. Gasljevic, G. Aguilar, and E. F. Matthys, "On two distinctive types of drag-reducing fluids, diameter scaling, and turbulent profiles," J. Non-Newtonian Fluid Mech. **96**, 405 (2001).
[36]V. K. Gupta, R. Sureshkumar, and B. Khomami, "Passive scalar transport in polymer drag-reducing turbulent channel flow," AIChE J. **51**, 1938 (2005).
[37]K. Gasljevic, G. Aguilar, and E. F. Matthys, "Buoyancy effects on heat transfer and temperature profiles in horizontal pipe flow of drag-reducing fluids," Int. J. Heat Mass Transfer **43**, 4267 (2000).
[38]K. Gasljevic, G. Aguilar, and E. F. Matthys, "An improved diameter scaling correlation for turbulent flow of drag-reducing polymer solutions," J. Non-Newtonian Fluid Mech. **84**, 131 (1999).
[39]G. Aguilar, "An experimental study of drag and heat transfer reduction in turbulent pipe flows for polymer and surfactant solutions," Ph.D. thesis, University of California at Santa Barbara, 1999.
[40]P. S. Virk and D. L. Wagger, "Aspects of mechanisms in type-B drag reduction," in *Structure of Turbulence and Drag Reduction, IUTAM Symposium*, Zurich, edited by A. Gyr (Springer-Verlag, Berlin, 1989), pp. 201–213.
[41]M. J. Rudd, "Velocity measurements made with a laser Doppler meter on the turbulent pipe flow of a dilute polymer solution," J. Fluid Mech. **51**, 673 (1972).
[42]K. Schmitt, P. O. Brunn, and F. Durst, "Scaling-up correlations for drag-reducing surfactants," in *Progress and Trends in Rheology 2: Proceedings of the Second Conference of European Rheologists*, Prague, June 17–20, 1986, edited by H. Gieskus *et al.* (Springer Verlag, Berlin, 1988).
[43]S. Rochefort and S. Middleman, "Effect of molecular configurations on Xanthan gum drag reduction," AIP Conf. Proc. **137**, 117 (1986).